ORIGINAL RESEARCH ARTICLE



Manufacturing of Complex NiTi Geometries with LPBF and Adapted Scanning Strategies

Sandra Herzig¹ · Medardus Eckert¹ · Linda Weisheit¹ · Bernhard Müller¹ · Stefan Holtzhausen² · Juliane Thielsch¹

Received: 20 February 2025 / Revised: 8 September 2025 / Accepted: 11 September 2025 © The Author(s) 2025

Abstract A binary Nickel-Titanium shape memory alloy was processed by Laser Powder Bed Fusion (LPBF) to manufacture lattice structures. The chemical composition of the powder was Ni_{50.9}Ti_{49.1} (at%) with the aim of obtaining pseudoelastic properties in the printed part. Adapted scanning strategies were chosen and used on a standard LPBF machine to achieve complex geometries with small, uniform feature sizes and a more precise modification of the local energy input. The as-built structures were analyzed with optical, thermal, and mechanical methods by means of optical microscopy, differential scanning calorimetry, and compression tests. The results demonstrate that LPBF combined with adapted scanning strategies can generate complex and homogeneous NiTi geometries (like metamaterials and programmable materials). Furthermore, the results show that scanning strategies have a significant influence on the thermal and therefore mechanical properties of the structures. We conclude that adapted scan strategies overcome the limitations of ordinary contour-hatch scan strategies and lead to shape memory properties which cannot be realized with conventional manufacturing techniques.

This article is an invited paper selected from presentations at the Shape Memory and Superelastic Technologies Conference and Exposition 2024, held May 6–10, 2024, in Cascais, Portugal, and has been expanded from the original presentation. The issue was organized by Dr. Parikshith Kumar, W. L. Gore & Associates, Inc., Prof. William LePage, University of Tulsa, and Dr. Harshad Paranjape, Confluent Medical Technologies.

Sandra Herzig
Sandra.herzig@iwu.fraunhofer.de

Published online: 19 October 2025

- Fraunhofer Institute for Machine Tools and Forming Technology IWU, Dresden, Germany
- ² TU Dresden, Mechanical Science and Engineering, Dresden, Germany

Keywords NiTi materials · Laser powder bed fusion · Lattice structures · Pseudoelasticity · As-built

Introduction

Nickel-Titanium (NiTi) is one of the most important shape memory alloys today due to its remarkable properties, which can be specifically tailored to meet particular functional requirements. NiTi, as a shape memory alloy, exhibits both the reversible shape memory effect and pseudoelasticity. These phenomena are related to a phase transformation between the low-temperature martensite phase and the high-temperature austenite phase which are characterized by the temperatures M_s , M_f , A_s , and A_f [1], respectively. These parameters define the temperatures where martensite and austenite start to transform (M_s, A_s) and where the phase transformation is completed (M_f, A_f) . Equivalent parameters are the phase transformation stresses where the phases begin to form and are fully formed. The relationship between transformation temperatures and transformation stresses follows the Clausius-Clapeyron equation. Consequently, the phase transformation between both phases can be stress- or temperature-induced.

The pseudoelastic properties of bulk NiTi are limited to around 8% strain [2]. Furthermore, machining of NiTi is a challenging task, making the manufacturing of complex geometries with very few undesirable impurities difficult to nearly impossible when using conventional manufacturing methods such as molding, forming, and subtractive manufacturing processes. As a result of the impediments, the material's full potential has not been harnessed and is still under investigation [2]. Laser Powder Bed Fusion (LPBF) has been demonstrated as a successful production route to realize geometries with a high degree of complexity [1, 3,



4]. It was shown that samples processed by LPBF can exhibit pseudoelastic behavior already in the as-built state [5] and that modifications of the processing parameters can change the properties of Ni-rich NiTi significantly [1, 6], which can be utilized intentionally to control the pseudoelastic properties of LPBF-manufactured NiTi.

Typical parameters for the adjustment of the functional and mechanical properties of NiTi are the laser parameters (e.g., laser power, scan speed, hatch spacing) and the scan parameters (scan pattern) [7], but an adjustment of the scan strategy is yet only common for bulk material [8, 9]. The use of adapted scan strategies for thin and delicate structures (like lattice structures) allows the scan parameters as additional parameters to modulate the properties of the final part.

The fabrication of porous and lattice structures using LPBF allows to attain specific properties. This is achieved not only by adjusting laser and scanning parameters but also by enabling the creation of specifically tailored feature sizes and geometrical designs, including unit cell design, the number and distribution of unit cells, and gradation [10, 11]. These geometrical structures extend beyond the designs of conventional unit cells (e.g., bcc unit cell), and, when combined with unique material behaviors such as pseudoelasticity, can result in extraordinary properties. The structures can range from metamaterials [12, 13] to programmable materials [14] that can execute a logical description. In this study, we will show the potential of adapted scan strategies for delicate NiTi structures (in this work with a feature size of around 200 um) in the as-built state and discuss the properties of complex LPBF-manufactured NiTi structures. In addition, we will present a structure with an incorporated mechanical element to enable the realization of specific properties, in our case a rapid change in stiffness under compression load. This work enhances the understanding of how modifications in scanning strategies, parameters, and lattice design affect the properties of NiTi manufactured using LPBF in the as-built state.

Materials and Methods

Sample Preparation

Gas-atomized Ni $_{50.9}$ Ti $_{49.1}$ (at%) powder (Nanoval GmbH & Co. KG) with particle sizes ranging from 15 to 45 μ m was utilized in a standard M2 cusing machine (Concept Laser GmbH). Figure 1 shows the particle size distribution and the metallographic analysis of the powder. The LPBF system contains a 400 W CW-diode-pumped fiber laser (-1070 nm) and was operated under argon atmosphere. The samples were fabricated on NiTi base plates, and a build space reduction of $90 \times 90 \times 120$ mm³ was implemented during fabrication. A layer thickness of 25 μ m, a laser focus diameter of

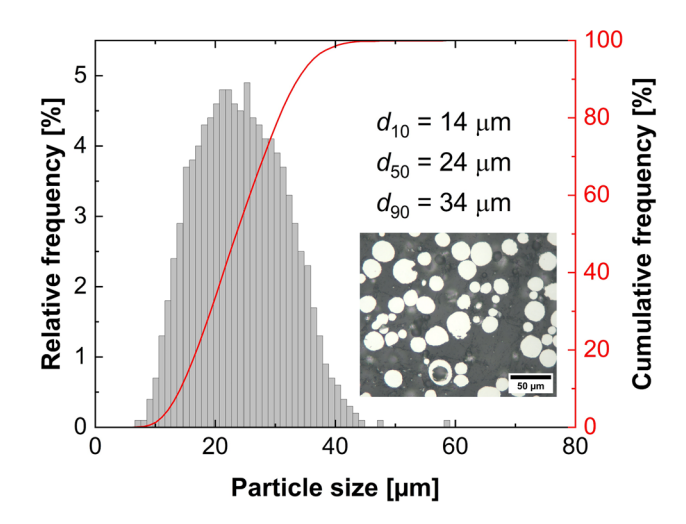


Fig. 1 Particle size distribution and metallographic image of the deployed NiTi powder

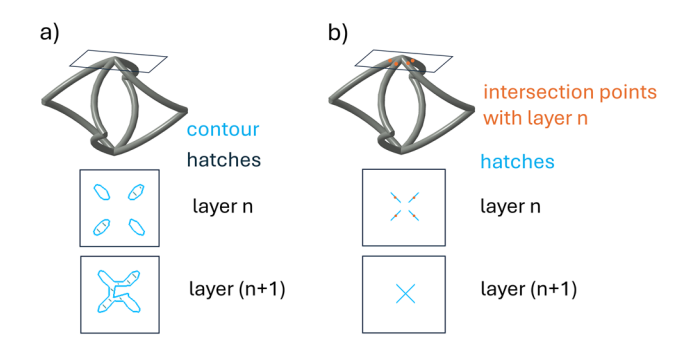


Fig. 2 Illustration of conventional scanning strategy (a) and adapted scanning strategy (b) of a unit cell

100 µm, a laser power of 200 W and a scanning speed of 500 mm/s were selected. The adapted scan strategy used in this work uses short scan vectors in each layer to represent a delicate feature instead of a contour and several hatches which conventional scan strategies [15] usually apply for bulk as well as thin structures. An example for the conventional and adapted scanning strategy pattern is shown in Fig. 2. The chosen vector configuration for the adapted scanning strategy was a line which means that every strut is only represented by one vector in form of a line which is shown in Fig. 2b. The vectors were oriented in the direction of the struts tilt direction and were adapted to the struts angle of inclination. As a result, flat struts are represented by longer vectors than steeper struts as vectors overlap less through adjacent layers for flatter struts. An essential difference during the preparation of the building process of adapted scan strategies compared to conventional scan strategies is that only a wireframe model is necessary during the slicing process for adapted scan strategies [16]. As a result, the feature size of the final part is not an information in the CAD model



and is therefore a result of the chosen laser and scan parameters. This also means that the same model can be used to generate the identical geometry with different feature sizes and doesn't need to get revised.

We manufactured a body-centered cubic lattice structure with a unit cell dimension of $a_x = a_y = a_z = 2.0$ mm once with conventional und once with adapted scan strategy to compare both scan strategies to each other. Next to body-centered cubic lattice structures, we investigated also bcc lattice structures with curved struts instead of straight ones. The lattice structure consisted of 4×4×4 unit cells and a unit cell dimension of $a_x = a_y = a_z = 2.6$ mm. An illustration of a complete sample is shown in Fig. 3a, b. One of these sample types features curved struts with an additional mechanical element within the unit cell to realize a rapid change in stiffness under compressive load. This additional mechanical element is positioned solely on one side of the unit cell and is aligned along the loading direction. As a result, the mechanical element experiences loading only beyond a certain strain threshold, once the contact gap between the outer struts and the element is bridged. Both sample types are shown in Fig. 3c, d.

Sample Characterization

For the optical analysis, the samples were examined using a digital microscope (Smartzoom 5, Carl Zeiss AG). Each sample was manually measured with the microscope's software tool to determine the average strut diameter (8 measurements) and the gap size between the outer cell and the inner mechanical element (5 measurements from different unit cells) from a side view. An additional microstructural analysis was performed with optical microscopy by embedding the lattice structure in resin. The embedded sample was

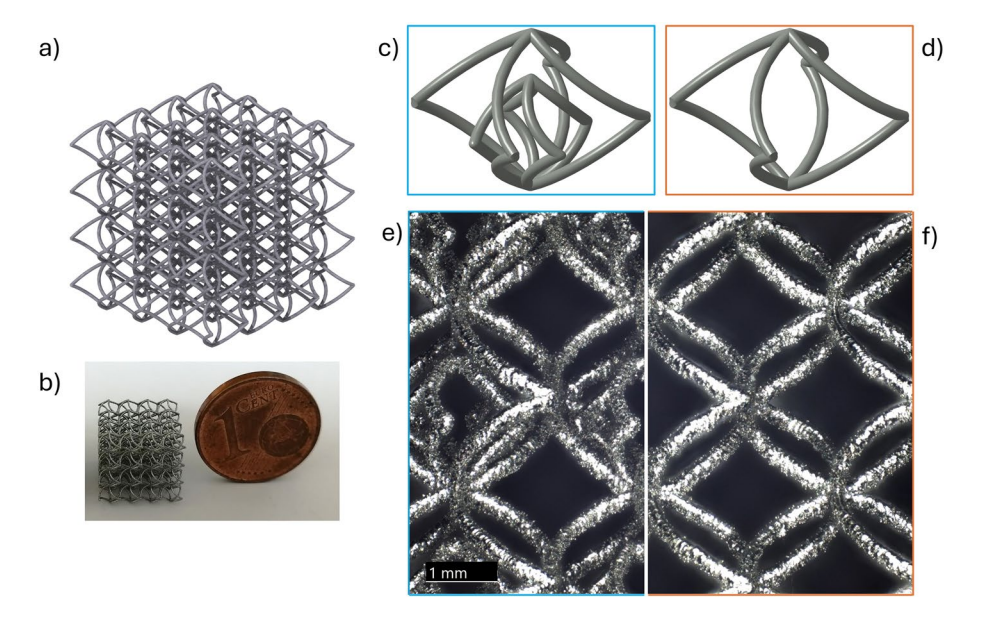
ground with sandpaper (P400 to P4000), polished with MasterMet-2 and etched with etchant consisting of $\rm H_20$, $\rm HNO_3$, and HF. The preparation result was documented with an Axioscope 7 (Carl Zeiss AG).

The particle size distribution of the powder was measured with dynamic picture analysis using a Camsizer X2. The morphology of the powder was investigated with light microscopy where the powder was embedded in resin and ground and polished as mentioned above. The powder investigations show that the particle size distribution fits the pre-defined range of particle sizes well, seen in Fig. 1. It is visible in the metallographic image that most particles have a sphericity near 1 which benefits a good flowability as it results in a high apparent density in the powder bed. However, there are also some hollow spheres and smaller satellites that were small enough to escape sorting during the sieving process prior to printing. Irregularly shaped particles or satellites reduce flowability, while hollow spheres can create pores in the final part.

The NiTi lattice structures were also investigated in terms of thermal and mechanical properties. The phase transformation temperatures were determined with a heat flow differential scanning calorimetry device (DSC) (Mettler Toledo DSC-3) by cutting several struts from the printed structures. The measurement cycle consisted of a cooling step to $-110~^{\circ}$ C, holding for 5 min at $-110~^{\circ}$ C, subsequent heating to 80 $^{\circ}$ C, holding for 5 min at 80 $^{\circ}$ C and cooling back to $-110~^{\circ}$ C. The temperature cycle was performed twice to eliminate any work hardening. The heating and cooling rate was set to 10 K/min. The powder was also analyzed via DSC to determine the phase transformation temperatures in the initial condition.

For the characterization of the mechanical properties, the samples were subjected to a cyclic compression test.

Fig. 3 Illustration (a) and photo (b) of a specimen, unit cell design with (c) and without mechanical element (d) and corresponding microscopic images of the unit cell with mechanical element (e) and without mechanical element (f)





The strain was measured via the traverse of the utilized material testing machine (FR020TN, ZwickRoell GmbH & Co. KG). The loading cell provided 1 kN. 5 N was chosen as a preload value. The samples were loaded up to 23% strain and unloaded down to 5 N for 10 cycles. The turning point of the strain was determined in a linear pre-test, with the strain rate set at 0.25%/s.

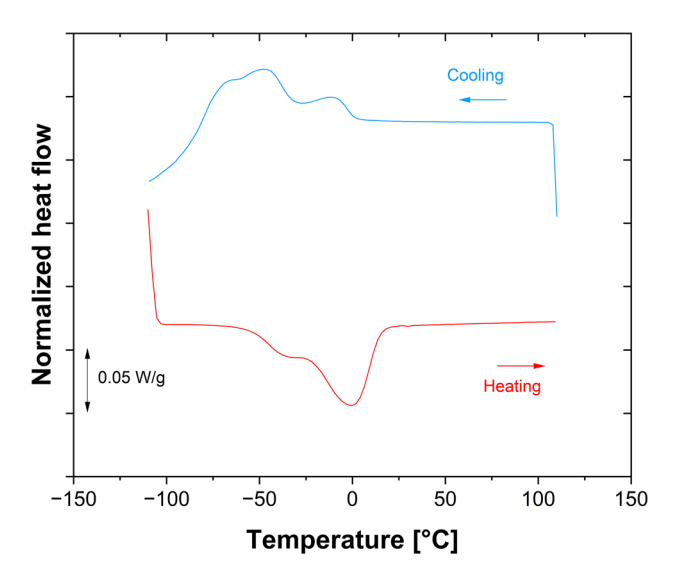
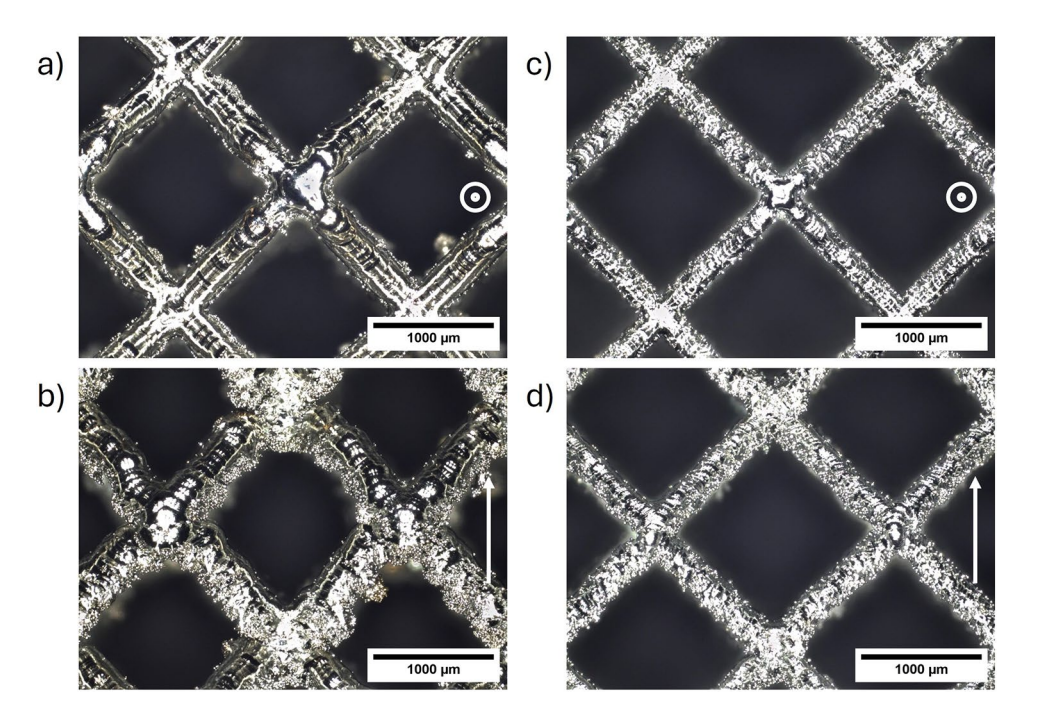


Fig. 4 DSC measurement of the used NiTi powder

Fig. 5 Microscopic images of NiTi-LPBF-manufactured bcc lattice structure with conventional (a, b) and adapted scan strategy (c, d), top view (a, c) and side view (b, d) are explained via arrows



Results and Discussion

A prerequisite for a suitable processing of NiTi powder to delicate lattice structures is suitable powder properties. The DSC measurement of the used powder is pictured in Fig. 4. The phase transformation temperatures of the powder were determined as $M_s = -82$ °C, $M_f = 1$ °C, $A_s = -53$ °C, and $A_f = 15$ °C which means it is possible to manufacture NiTi samples with a A_f temperature below room temperature with the powder [17]. Nevertheless, the powder shows multiple transformation peaks which indicate that the powder composition isn't homogeneous [8]. The kinetic barrier for the martensitic phase transformation is higher than for the austenitic and R-phase transformation which results in a greater thermal range during the cooling phase for R stability [18]. The measurement for the powder doesn't show this regulation which is why the assumption of the heterogeneous powder composition was chosen. The powder analysis concludes that the powder is suitable for additive manufacturing of NiTi parts with phase transformations below room temperature, but minor defects can't be prevented due to the present powder morphology.

A body-centered cubic unit cell manufactured with conventional and adapted scan strategy is shown in Fig. 5 with the printing direction perpendicular (Fig. 5a, c) and parallel (Fig. 5b, d) to the picture plane. The adapted can strategies were developed because the conventional approach results in several limitations because of its relatively high energy input for thin structures. Some of them are the challenge to manufacture inclination angles below 20° [19] and the minimal feature size which is material-dependent and 200–300 µm



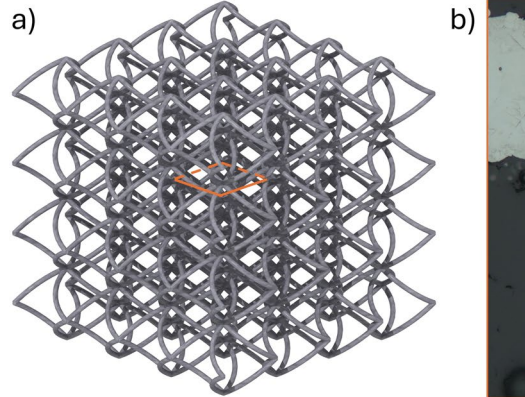
for Ti-6Al-4V [20, 21]. The minimal feature size was not yet specifically acquired for NiTi and the determination is not part of this work which is why the value for Ti-6Al-4V was mentioned here. The adapted scan strategy is able to overcome several limitations of conventional scan strategies [16, 22]. The smallest possible feature size for adapted scan strategies is around the laser beam diameter [16]. Gustmann et al. [23] were able to realize a feature size of 130 µm with this scan strategy with a laser beam diameter of 100 µm for NiTi. Other advantages are that inclination angles down to 10° can be easily manufactured, the energy input is more homogeneous as the scan strategy is symmetric for symmetric geometries and the shorter overall vector length results in a faster building process etc. [16, 22]. The differences in symmetry and vector length between conventional and adapted scan strategies are already visible in Fig. 2. The adapted scan strategies implement furthermore better surface qualities for small features [16, 22]. A contour with suitable laser parameters realizes a decent surface quality for thicker features but features which are just several powder particles thick are more exposed to a lot of powder adhesions (compared to the small feature sizes). Figure 5 emphasizes several other of these statements by showing that the conventional scan strategy resulted in a bigger feature size, a higher quantity of fused particles, more heterogeneous distributed powder adhesions, more non-uniform struts and a higher energy input in the nodes compared to the adapted scan strategy. The different CAD models inhibit a comparison between targeted and manufactured feature size as the feature size is not an information of the wireframe model of the adapted scan strategy. We compared the quality of printed features by means of inclined features as vertical (to the base plate) printed features are known for only a modest quantity of powder adhesions because especially downside areas of LPBF-manufactured parts tend to high amounts of fused powder particles. This means that laser and scan parameters can result in a proper surface quality for vertical features but in plenty and heterogeneously distributed powder adhesions for inclined features. For this reason, a better method to check different laser and scan parameters against each other is to compare inclined features with the same angle of inclination which is shown with the body-centered cubic structure in Fig. 5. As a conclusion of the comparison, we prefer the adapted scan strategy for thin and delicate structures which are used in this work.

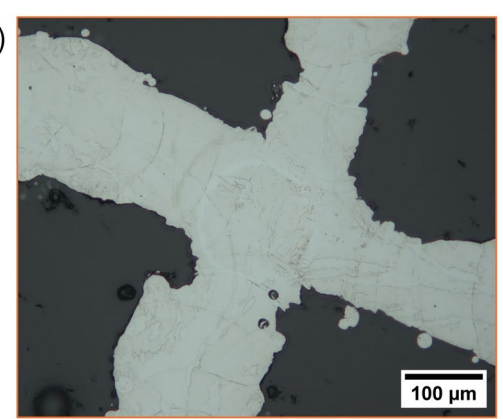
The microscopic images of the unit cells with curved struts which were additively manufactured with the adapted scan strategy are presented in Fig. 3e, f. The unit cell with the mechanical element is shown in Fig. 3e while the reference cell without the element is displayed in Fig. 3f. Microscopic analysis revealed an average strut diameter of (199±7) μm. The gap between outer cell and mechanical element had a size of (490 ± 16) µm. Since LPBF is a powder-based additive manufacturing technique, it results in powder adhesions, particularly on overhang surfaces which is noticeable in the as-built condition. It is also evident that the scanning strategy achieves a good connectivity between the adjacent layers. To support this observation, an optical microscope image of a node and its adjoining struts is presented in Fig. 6. The fusion of the individual scan paths within the struts and in the node and therefore the connectivity is visible. Also, some pores exist but no preferential region for pores within the geometry or unit cell could be detected. In general, the micrograph shows the typical heterogeneous microstructure, with visible scan paths resulting from the locally repetitive melting and solidifying processes.

Adapted scanning strategies support a more precise adjustment of the energy input which contributes to improved quality and properties of the final parts.

Functional and structural properties such as strut diameter and structural quality can be tailored by the chosen laser parameters (e.g., laser power, scanning speed) and scanning strategy parameters (e.g., number of vectors, vector orientation, vector length). Figure 7 shows the influence of the line vector length (v_L) on the phase transformation temperatures for constant laser parameters. The results demonstrate the behavior for a body-centered cubic lattice with straight struts as this design displays a constant inclination angle

Fig. 6 Inset to indicate the position in the lattice specimen (a) and corresponding microscopic image showing a node of a NiTi-LPBF lattice structure (b)







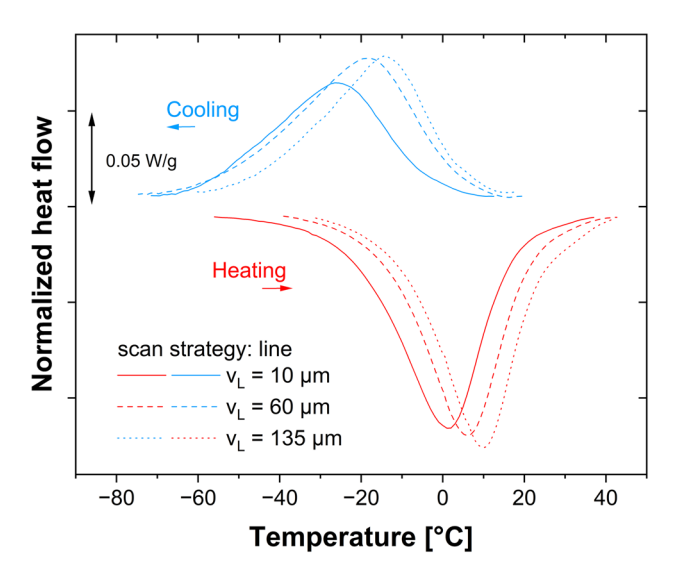


Fig. 7 DSC measurements of NiTi lattice structures with adapted scanning strategy (line) for different vector lengths

which results in a defined vector overlap between adjacent layers for a specific vector length. The results indicate that the phase transformation temperatures rise as the line vector length increases. A longer line vector correlates to a higher energy input because the laser exposure time is extended at the same scanning speed. Additionally, for inclined struts, a longer vector length results in greater overlap of successive vectors in adjacent layers, which is associated with a higher proportion of remelted and re-solidified microstructure.

The transformation temperatures for Ni-rich compositions are strongly dependent on the Ni-Ti ratio [24]. Therefore, higher energy input leads to elevated phase transformation temperatures, as the increased energy raises the likelihood of nickel evaporation due to its lower evaporation temperature compared to titanium [17]. Consequently, structures fabricated with a larger vector length may experience a depletion of nickel in the matrix, which ultimately results in an increase in the transformation temperatures. We must keep in mind that these findings were generated for lattices with straight struts, where the vector length for the struts is constant throughout the building job. When fabricating lattices with a more complex structure, we will encounter varying inclination angles in the building direction, which results in non-uniform vector lengths throughout the structures. Therefore, we assume a broader range of transformation temperatures within a single lattice.

The average phase transformation temperatures for the lattice structures are M_f = -61 °C, M_s =5 °C, A_s = -27 °C, and A_f =28 °C for the structure with the mechanical element and M_f = -64 °C, M_s =4 °C, A_s =-26 °C, and A_f =23 °C for the structure without the mechanical element. The A_f temperatures indicate the presence of primarily austenite at room temperature. The phase transformation temperatures

Table 1 Phase transformation temperatures of powder and lattice structures with adapted scan strategy

	$M_f(^{\circ}\mathrm{C})$	<i>M</i> _s (°C)	<i>A_s</i> (°C)	$A_f(^{\circ}C)$
Powder	-82	1	-53	15
Lattice structure with mechanical element	-61	5	-27	28
Lattice structure without mechani- cal element	-64	4	-26	23

indicate a broad transformation range which was to be expected as additive manufacturing results in heterogeneous microstructure in the as-built state (Fig. 6) which in turn results in broad transformation peaks [25]. Both samples have higher phase transformation temperatures than the initial powder which is show in Table 1. The processing with the laser beam usually results in higher temperatures compared to the powder because the energy leads to nickel evaporation which in return increases the temperatures [17, 24] like explained above. The additional mechanical element is accompanied by a greater number of scan vectors per unit cell. Consequently, the two different lattice structures exhibit varying distributions of the number of scan vectors relative to the scan vector length. The additional mechanical element increases the number of struts that can extend from a node, resulting in a locally higher energy input as more vectors are concentrated in the small node area. This may explain the slight differences in the transformation temperatures of the two structures.

Figure 8 shows the stress-strain curve under compression for both lattice structures. The curve progressions illustrate the typical linear elastic and pseudoelastic regions, and further indicate that the combination of NiTi with a lattice structure featuring a mechanical element can achieve programmable stiffness behavior. The point at which stiffness increases is primarily determined by the geometry. Both lattice structures achieve nearly reversible effective strains of 20%, demonstrating the potential of complex NiTi (lattice) structures as this behavior is not feasible with bulk NiTi geometries. Both curve progressions display an initially higher proportion of plastic deformation in the first cycle and a decreasing increment of plastic deformation as the number of cycles increases. This behavior has been denoted as transformation ratcheting [26]. This term describes the cyclic accumulation of strain due to the accumulation of remaining martensite resulting from incomplete phase transformation from stressinduced martensite to austenite [26]. It is also referred to as functional fatigue of pseudoelastic NiTi shape memory alloys and the degeneration of pseudoelasticity during



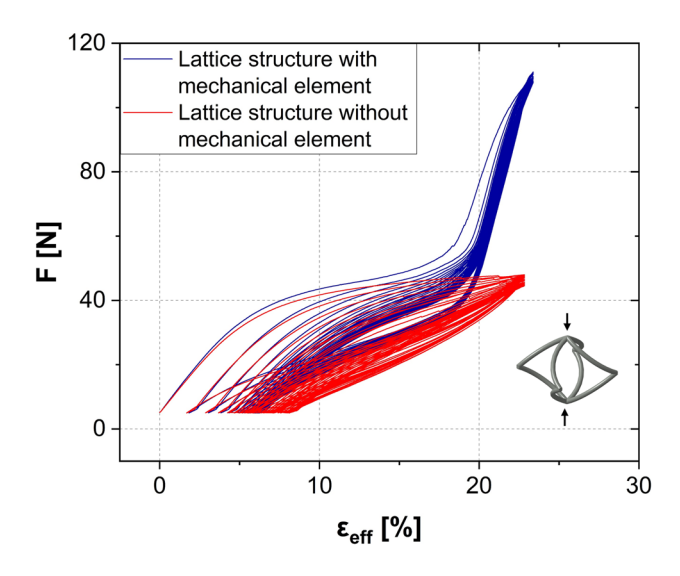


Fig. 8 Force-strain curves under compression load for NiTi unit cell structure with and without mechanical element

cyclic deformation [27]. The increase in plastic strain, the decrease in transformation stress and the dissipation of energy are a result of the transformation ratcheting, whereby all gradients decrease with the number of cycles, and the values approach a constant value over time [26, 28]. The unloading part of the curves in Fig. 8 illustrates a different increase in plastic deformation. For the initial five cycles, the structure without a mechanical element exhibits lower non-reversible deformation. However, at the beginning of the sixth cycle, the structure with the mechanical element displays smaller plastic deformation. One explanation for the higher plastic deformation of the lattice structure with mechanical element in the first few cycles is that several nodes of the structure experience a higher energy input due to the increased number of struts. Consequently, the phase transformation temperature in the struts can be locally higher, leading to minimally higher transformation temperatures for the overall structure, as mentioned above. Due to possible higher transformation temperatures, the proportion of residual martensite in the sample with mechanical element is higher after unloading than for the structure without additional mechanical element. This order reverses after five cycles, and the structure with the mechanical element exhibits a lower proportion of accumulated residual strain compared to the structure without the mechanical element. An explanation for this behavior is that the structure with mechanical element distributes the load at higher strains across more struts, which results in lower local deformation in this sample type. Consequently, the increase in plastic deformation is lower, and the absolute effective plastic strain per cycle falls below that of the lattice structure without the mechanical element.

Conclusion

LPBF enables the fabrication of complex NiTi structures with pseudoelastic properties in the as-built state. The approach of an adapted scanning strategy, which uses fewer scan vectors and shorter scan lengths to melt a structure compared to conventional scanning strategies, has been successfully applied to complex NiTi geometries, resulting in good connectivity in the struts and nodes despite the shorter scan lengths. The chosen parameters resulted in feature sizes of about 200 µm, which can be altered by changing the laser focus, laser parameters and scan strategy parameters. Regardless of the selected manufacturing parameters, complex LPBF structures will always exhibit powder adhesions in the as-built state, as these are unavoidable on downside surfaces. The optimization of parameters will only minimize the amount but not fully prevent the formation. NiTi is very sensitive to the amount and kind of energy input. As a result, the mechanical behavior of LPBF-NiTi structures can be influenced by the laser parameters, scanning strategy, and geometry parameters, while the functional properties are primarily affected by the laser parameters and scanning strategy concurrently. The pseudoelasticity of the material allows for unprecedented behavior within the elastic region, which can be repeatedly achieved over many cycles. This was shown with the example of a unit cell lattice structure which changes its stiffness behavior under compression. The displayed structure can, for instance, be implemented in a planar clamping element that allows for adjustments to different shapes due to its high and low stiffness in varying strain ranges. The manufacturing of such unique NiTi lattice structures pushes the boundaries of NiTi specifications, leading to extraordinary material characteristics.

Further investigations are necessary to evaluate the interactions between process parameters, scanning strategy, and geometry parameters in greater detail, as the topic and its insights still exhibit deficits. Advancements in geometry also present the opportunity to create more sophisticated mechanical properties. Additively manufactured samples experience, in the as-built state, a heterogeneous energy input, resulting in a heterogeneous microstructure due to the layer-by-layer structure. As a result, features with different inclination angles do not exhibit completely identical properties, as the energy input and the proportion of remelted material vary for each geometry parameter (inclination angle etc.). A numerical analysis for the investigated lattice structures is also part of further work to determine the local strain and strain distribution.



Acknowledgments This research was carried out under financial support granted by Fraunhofer Cluster of Excellence Programmable Materials (Fraunhofer CPM) under the project title "Generativgefertigte metallische Metamaterialien" and constructive projects.

Funding Open Access funding enabled and organized by Projekt DEAL.

Data availability The datasets generated and analyzed during the study are not publicly available due to institutional restrictions, but are available from the corresponding author on reasonable request.

Open Access This article is licensed under a Creative Commons Attribution 4.0 International License, which permits use, sharing, adaptation, distribution and reproduction in any medium or format, as long as you give appropriate credit to the original author(s) and the source, provide a link to the Creative Commons licence, and indicate if changes were made. The images or other third party material in this article are included in the article's Creative Commons licence, unless indicated otherwise in a credit line to the material. If material is not included in the article's Creative Commons licence and your intended use is not permitted by statutory regulation or exceeds the permitted use, you will need to obtain permission directly from the copyright holder. To view a copy of this licence, visit http://creativecommons.org/licenses/by/4.0/.

References

- Haberland C, Elahinia M, Walker JM, Meier H, Frenzel J (2014)
 On the development of high quality NiTi shape memory and
 pseudoelastic parts by additive manufacturing. Smart Mater
 Struct. https://doi.org/10.1088/0964-1726/23/10/104002
- Bellouard Y (2008) Shape memory alloys for microsystems: a review from a material research perspective. Mater Sci Eng A 481–482:582–589
- Haberland C (2012) Additive Verarbeitung von NiTi-Formgedächtniswerkstoffen mittels Selective Laser Melting, Ph.D. Thesis, Available from Ruhr University Bochum Library, Germany. Thesis completed
- Dadbakhsh S, Speirs M, Humbeeck JV, Kruth J-P (2016) Laser additive manufacturing of bulk and porous shape-memory NiTi alloys: from processes to potential biomedical applications. MRS Bull 41(10):765–774
- Moghaddam NS, Saedi S, Amerinatanzi A, Hinojos A, Ramazani A, Kundin J, Mills MJ, Karaca H, Elahinia M (2019) Achieving superelasticity in additively manufactured NiTi in compression without post-process heat treatment. Sci Rep. https://doi.org/10.1038/s41598-018-36641-4
- Frenzel J, George EP, Dlouhy A, Somsen C, Wagner MF-X, Eggeler G (2010) Influence of Ni on martensitic phase transformations in NiTi shape memory alloys. Acta Mater. https:// doi.org/10.1016/j.actamat.2010.02.019
- Elahinia M, Andani NT, Safaei K, Poorganji B (2023) Rotationg scanning strategies for tailoring crystallographic texture of additively manufactured NiTi shape memory alloy. Mater Lett. https://doi.org/10.1016/j.matlet.2023.134156
- Wang X, Yu J, Liu J, Chen L, Yang Q, Wie H, Sun J, Wang Z, Zhang Z, Zhao G, Van Humbeeck J (2020) Effect of process parameters on the phase transformation behavior and tensile properties of NiTi shape memory alloys fabricated by selective laser melting. Addit Manuf. https://doi.org/10.1016/j.addma. 2020.101545

- Xiong Z, Li Z, Sun Z, Hao S, Yang Y, Li M, Song C, Qiu P, Cui L (2019) Selective laser melting of NiTi alloy with superior tensile property and shape memory effect. J Mater Sci Technol. https://doi.org/10.1016/j.jmst.2019.05.015
- Saedi S, Turabi AS, Andani MT, Haberland C, Elahinia M, Karaca H (2016) Thermomechanical characterization of Ni-rich NiTi fabricated by selective laser melting. Smart Mater Struct. https://doi.org/10.1088/0964-1726/25/3/035005. (m)
- Sun L, Chen K, Geng P, Zhou Y, Wen S, Shi Y (2023) Mechanical and shape memory properties of NiTi triply periodic minimal surface structures fabricated by laser powder bed fusion. J Manuf Process 101:2091–2200
- Eggeler G, Hornbogen E, Yawny A, Heckmann A, Wagner M (2004) Structural and functional fatigue of NiTi shape memory alloys. Mater Sci Eng A 378:24–33
- Jiang D, Thissen H, Hughes TC, Yang K, Wilson R, Murphy AB, Nguyen V (2024) Advances in additive manufacturing of auxetic structures for biomedical application. Mater Today Commun 40:110045
- Scalet G (2024) Programmable materials: current trends, challenges, and perspectives. Appl Mater Today. https://doi.org/10.1016/j.apmt.2024.102372
- Korn H, Koch P, Kordaß R, Holtzhausen S, Schöne C, Müller B, Stelzer R (2018) Adapted scan strategy and slicing tool for improvement of strut precision in lattice structures. ASPE and euspen summer topical meeting: advancing precision in additive manufacturing, 50
- Korn H, Holtzhausen S, Koch P, Seidler A, Gebhardt F, Thielsch J, Drossel W-G (2022) Scanstrategien: ein Enabler für filigrane Bauteile auf bestehender LPBF-Anlagentechnik. Proceedings of the 18th Rapid.Tech 3D Conference Erfurt, Germany, 17–19 May 2022. https://doi.org/10.3139/9783446475281.009
- Chen W, Gu D, Yang J, Yang Q, Chen J, Shen X (2022) Compressive mechanical properties and shape memory effect of NiTi gradient lattice structures fabricated by laser powder bed fusion. Int J Extrem Manuf. https://doi.org/10.1088/2631-7990/ac8ef3
- Duerig TW, Bhattacharya K (2015) The influence of the R-phase on the superelastic behavior of NiTi. Shape Mem Superelasticity 1:153–161
- Mazur M, Leary M, Sun S, Vcelka M, Shidid D, Brandt M (2016) Deformation and failure behaviour of Ti-6Al-4V lattice structures manufactured by selective laser melting (SLM). Int J Adv Manuf Technol 84:1391–1411
- Maconachie T, Leary M, Lozanovski B, Zhang X, Qian M, Faruque O, Brandt M (2019) Slm lattice structures: properties, performance, applications and challenges. Mater Des. https:// doi.org/10.1016/j.matdes.2019.108137
- Aktas A, Caprio L, Galbusera F, Previtali B, Demir AG (2022) Coordination of spatial and temporal laser beam profile towards ultra-fine feature fabrication in laser powder bed fusion. J Addit Manuf Technol. https://doi.org/10.18416/JAMTECH.2212687
- Korn H, Koch P, Bittner F, Kordaß R, Holtzhausen S, Müller B, Schöne C, Stelzer R (2018) CAD-integrierte Schichtdatenerzeugung für feine Gitterstrukturen und Bestimmung geeigneter Fertigungsparameter für Laser-Strahlschmelzen. Proceedings of the 15th Rapid.Tech Conference Erfurt, Germany, 5–7 June 2018. https://doi.org/10.3139/9783446458123.023
- Gustmann T, Gutmann F, Wenz W, Koch P, Stelzer R, Drossel WG, Korn H (2020) Properties of a superelastic NiTi shape memory alloy using laser powder bed fusion and adaptive scanning strategies. Prog Addit Manuf 5(1):11–18
- Frenzel J, George EP, Dlouhy A, Somsen C, Wagner MF-X, Eggeler G (2010) Influence of Ni on martensitic phase transformations in NiTi shape memory alloys. Acta Mater 58(9):3444–3458



- Lu HZ, Ma HW, Luo X, Wang Y, Wang J, Lupoi R, Yin S, Yang C (2021) Microstructure, shape memory properties, and in vitro biocompatibility of porous NiTi scaffolds fabricated via selective laser melting. J Mater Res Technol 15:6797–6812
- Kang G, Kan K, Qian L (2009) Liu, Y: Ratchetting deformation of super-elastic and shape-memory NiTi alloys. Mech Mater 41:139–153
- Freeman FSHB, Jones LM, Goodall AD, Ghadbeigi H, Todd I (2024) Structural metamaterial lattices by laser powder-bed fusion of 17–4PH steel. Additive Manufacturing Letters. https://doi.org/10.1016/j.addlet.2023.100190
- 28. Yu C, Kang G, Song D, Kan Q (2015) Effect of martensite reorientation and reorientation-induced plasticity on multiaxial transformation ratchetting of super-elastic NiTi shape memory alloy: new consideration in constitutive model. Int J Plast 67:69–101

Publisher's Note Springer Nature remains neutral with regard to jurisdictional claims in published maps and institutional affiliations.

